SCIENCE CHINA Materials ARTICLES

mater.scichina.com link.springer.com

Published online 10 September 2018 | https://doi.org/10.1007/s40843-018-9338-6

Sci China Mater 2019, 62(4): 465–473

Facile fabrication of interconnected-mesoporous T-Nb_2O_5 nanofibers as anodes for lithium-ion batteries

Linzhen Lou[1†], Xiangzhong Kong[1†], Ting Zhu[1], Jiande Lin[1], Shuquan Liang[1], Fei Liu[1], Guozhong Cao[1,2] and Anqiang Pan[1*]

ABSTRACT **Niobium pentoxide (Nb_2O_5) has been extensively studied as anode materials for lithium ion batteries (LIBs) due to its good rate performance and safety advantages. However, the intrinsic low electronic conductivity has largely restricted its practical application. In this work, we report the construction of mesoporous T-Nb_2O_5 nanofibers by electrospinning followed by heat treatment in air. The interconnected mesoporous structure ensures a high surface area with easy electrolyte penetration. When used as anodes for LIBs, the mesoporous Nb_2O_5 electrode delivers a high reversible specific capacity of 238 mA h g^{-1} after 1,000 cycles at a current density of 1 A g^{-1} within a voltage range of 0.01–3.0 V. Even at a higher discharge cut-off voltage window of 1.0–3.0 V, it still possesses a high reversible capacity of 166 mA h g^{-1} after 200 cycles. Moreover, the porous Nb_2O_5 electrode also exhibits excellent rate capability. The enhanced electrochemical performances are attributed to the synergistic effects of porous nanofiber structure and unique crystal structure of T-Nb_2O_5, which has endowed this material a large electrode-electrolyte contact area with improved electronic conductivity.**

Keywords: T-Nb_2O_5, interconnected-mesoporous nanofibers, electrospinning, lithium ion batteries

INTRODUCTION

Lithium-ion batteries (LIBs) are considered to be one of the most promising power sources for electronic devices because of their high energy density, no memory effect, little self-discharge and environmental benignity [1–3]. As a low-cost material, graphite is the most widely used anode so far due to its good conductivity and stable physical properties. Unfortunately, its immanent drawbacks, such as low energy and power density, poor rate capacity, limited cycle life, and safety issues, have largely restricted its future utilization in LIBs [4–6]. Thus, it is imperative to develop alternative anode materials to address the above issues for next-generation high-performance LIBs.

Recently, some metal oxides MO_x (M=Co, Ni, Mn, Cu, Fe, Sn) have attracted intensive attentions for LIBs because of their high theoretical capacity, abundant sources and environmental benignity [7–9]. However, the MO_x electrodes usually suffer from a huge volume expansion during the insertion and extraction of lithium ions (Li^+), resulting in a severe irreversible capacity loss and poor cycling capability, which is unfavorable to their large-scale commercialization [10–14]. Among these, niobium pentoxide (Nb_2O_5) has been widely studied because of its slight volume changes upon cycling and high lithiation potential (1.0–2.0 V *vs.* Li/Li^+). The unique lithiation potential which is higher than that of the formation voltage of solid electrolyte interface (SEI) can suppress lithium dendrite deposition on the electrode surface, thereby relieving electrode pulverization and improving safety and cycling capability [15,16]. As reported, Nb_2O_5 has a class of polymorphic forms, including amorphous (*a*-Nb_2O_5), orthorhombic (T-Nb_2O_5), pseudo hexagonal (TT-Nb_2O_5) and monoclinic (M-Nb_2O_5) [17–19]. The previous electrochemical results have suggested that T-Nb_2O_5 possesses a good battery performance owing to its unique properties such as layered structure, high chemical stability and open intrinsic framework [20]. Nonetheless, the poor intrinsic electrical conductivity

[1] School of Materials Science & Engineering, Central South University, Changsha 410083, China
[2] Department of Materials Science & Engineering, University of Washington, Seattle 98195, USA
[†] These authors contributed equally to this work.
[*] Corresponding author (email: pananqiang@csu.edu.cn)

(3×10^{-6} S cm^{-1}) results in a sluggish Li^+ diffusivity, leading to the poor cycling stability and rate capacity [21].

The common strategies to address the abovementioned issues are to enhance intrinsic electronic/ionic conductivity and reduce the diffusion length for ions/electrons within the electrode. Carbon coating is an efficient way to improve the conductivity of electrode materials, which has been previously reported in LIBs. For examples, Kim *et al.* [22] has prepared Nb_2O_5/carbon electrode, which exhibits a stable cycle life and outstanding rate capability. However, the specific capacity is not satisfactory. Construction of nanostructured materials can also enhance the electrochemical performances. Through downsizing the particle size to nanoscale, materials could show higher surface area, which can improve the interface between the electrode and electrolyte so as to shorten the diffusion pathway of electrons and ions. To date, various Nb_2O_5 nanostructures have been synthesized, such as nanobelts [23], nanotrees [24], nanosheets [25] and nanowires [26,27]. Particularly, 1D nanomaterials with the merits of short ion diffusion distance, facile electron transportation channel and quick electrolyte infiltration have received more research attentions [28]. For example, Liu and co-workers [29] synthesized 1D Nb_2O_5 nanobelts, which exhibit a reversible capacity of 95.8 mA h g^{-1} after 200 cycles at 1 A g^{-1} in a voltage range of 1.0–3.0 V. However, the long-term cycling stability and rate capability of these simplex nanostructures are still far from satisfaction for the industrial use [30,31]. Fabrication of nanomaterials with porous structure could further provide more active sites, decrease the diffusion length and facilitate electrolyte penetration. Meanwhile, the void space in the porous structure can buffer the volume change upon cycling, which is helpful to keep the structural integrity of electrodes during cycling [32,33]. Sasidharan *et al.* [34] synthesized Nb_2O_5 hollow nanospheres with a high capacity of 172 mA h g^{-1} after 250 cycles at 0.2 A g^{-1}. Rahman *et al.* [5] designed vein-like nanoporous network of Nb_2O_5 electrodes, which exhibited greatly improved rate performance. Till now, Nb_2O_5 with 1D porous structure has rarely been reported yet.

In this work, we reported interconnected-mesoporous T-Nb_2O_5 nanofibers *via* electrospinning followed by calcination process. The obtained nanofibers are of high porosity and the mesopores are interconnected with one another. When used as anodes for LIBs, this material exhibited excellent electrochemical performances in the voltage ranges of 0.01–3.0 V and 1.0–3.0 V, including good rate capabilities and long-term cycling stabilities.

EXPERIMENTAL SECTION

Synthesis of Nb_2O_5 porous nanofibers

All the solvents and chemicals were of analytical grade and used without further purification. A solution was prepared by dissolving 0.025 mmol niobium hydroxide oxide ($H_5Nb_3O_{10}$) and 0.225 mmol oxalic acid dehydrate ($H_2C_2O_4{\cdot}2H_2O$) in 1 mL of deionized water under magnetic stirring at 80°C for 10 min. Then the above solution was added into 9 mL of *N*,*N*-dimethylformamide (DMF), followed by the addition of 1 g of polyvinylpyrrolidone (PVP) under magnetic stirring at room temperature to form a homogeneous transparent viscous solution. Subsequently, the well-mixed electrospinning solution was transferred into a 10 mL plastic syringe with a 20-gauge stainless steel needle positioned 15 cm away from the collector. During the process, the applied direct current (DC) voltage was 12 kV and the solution flow rate was kept constant (0.4 mL h^{-1}). The as-synthesized precursors were collected on the aluminum foil wrapped around the rotating drum. After that, the porous Nb_2O_5 nanofibers were obtained by annealing the precursors at 600°C in air for 2 h with a heating rate of 2°C min^{-1}.

Materials characterization

The crystal structure of the samples was confirmed by powder X-ray diffraction (XRD) measurements using the Rigaku D/max 2500 X-ray diffractometer (Cu Kα radiation, λ=1.54178 Å). The thermal behavior of the obtained precursors was conducted from ambient temperature to 800°C at a heating rate of 10°C min^{-1} in air on a combined thermogravimetric (TG) and differential scanning calorimetry (DSC) analysis instrument (Netzsch STA 449C, Germany). The morphologies and structures of the samples were characterized by field-emission scanning electron microscopy (FESEM, FEI Nova NanoSEM 230) and high-resolution transmission electron microscope (HRTEM, FEI Tecnai G2 F20). Nitrogen adsorption-desorption isotherm measurements were performed on a Micromeritics ASAP 2460 to study the specific surface area and pore-size distribution of the samples.

Electrochemical measurement

The electrochemical measurements were carried out in CR2016 type coin cells. The electrode materials were mixed with super-P and sodium carboxymethyl cellulose (CMC) at the weight ratio of 80:10:10 in distilled water to form slurry, which was coated on copper foil followed by drying in a vacuum oven at 80°C for 12 h. The mass loading of the active material was around 1 mg cm^{-2}. All

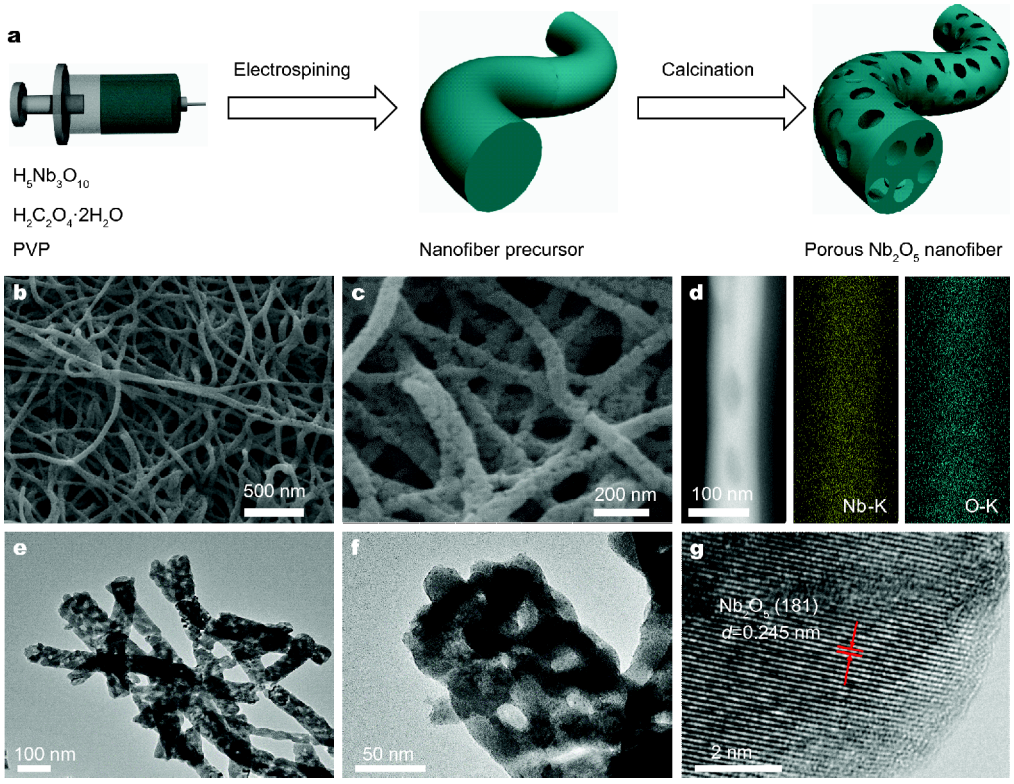

Figure 1 The illustration of the formation process of porous Nb_2O_5 nanofibers (a); SEM (b, c), elemental mapping (d) and TEM (e–g) images of the porous Nb_2O_5 nanofibers after heat treatment.

the half-cells were assembled into 2016-type coin cells in a glovebox filled with ultrahigh purity argon using lithium metal as counter and reference electrodes, and 1 mol L^{-1} $LiPF_6$ in ethylene carbonate/dimethyl carbonate/ethylmethyl carbonate (EC/DMC/EMC) (1:1:1, vol%) as the electrolyte. The galvanostatic charge/discharge tests were carried out on a Land battery tester (Land CT 2001A, Wuhan, China). The cyclic voltammetry (CV) measurement was tested on an electrochemical workstation (CHI660C, China) at a scan rate of 0.1 mV s^{-1} in the potential range of 0.01–3.0 V and 1.0–3.0 V (*vs.* Li^+/Li). The electrochemical impedance spectrometry (EIS) was performed on an AUTOLAB electrochemical station (Metrohm, Netherlands) in the frequency range of 100 kHz to 10 mHz. All the electrochemical tests were performed at room temperature.

RESULTS AND DISCUSSION

The overall fabrication process of the interconnected-mesoporous Nb_2O_5 nanofibers is illustrated in Fig. 1a. Briefly, a homogeneous solution of niobium hydroxide oxide, oxalic acid and PVP was electrospun into nanofiber precursors. Then, the precursors were thermally treated at 600°C in air for 2 h to obtain mesoporous Nb_2O_5 nanofibers. During the calcination process, the niobium oxalates were *in-situ* transformed into Nb_2O_5, whereas interconnected-mesoporous were formed as a result of the pyrolysis of polymer. The morphology and nanostructure of the porous nanofibers were characterized by SEM and TEM. SEM images in Fig. S1 shows the morphology of the as-spun precursors. The precursor nanofibers are highly uniform with a diameter of ~100 nm and show a smooth surface. Fig. 1b shows the SEM image of the as-synthesized Nb_2O_5 nanofibers derived from the as-spun fiber precursor. It reveals that the nanofiber structure is well preserved with the diameters unaltered, suggesting the structural robustness of these 1D nanostructures. A higher magnification (Fig. 1c) further reveals that a rough surface of the fibers and numerous pores can be observed clearly, which could be ascribed to the oxidation or decomposition of the polymers and niobium oxalates during the calcination process. Fig. 1d shows the elemental mapping of the mesoporous Nb_2O_5 nanofibers, where Nb and O are homogeneously distributed along the 1D structure. The further TEM images (Fig. 1e–g) have further reflected the

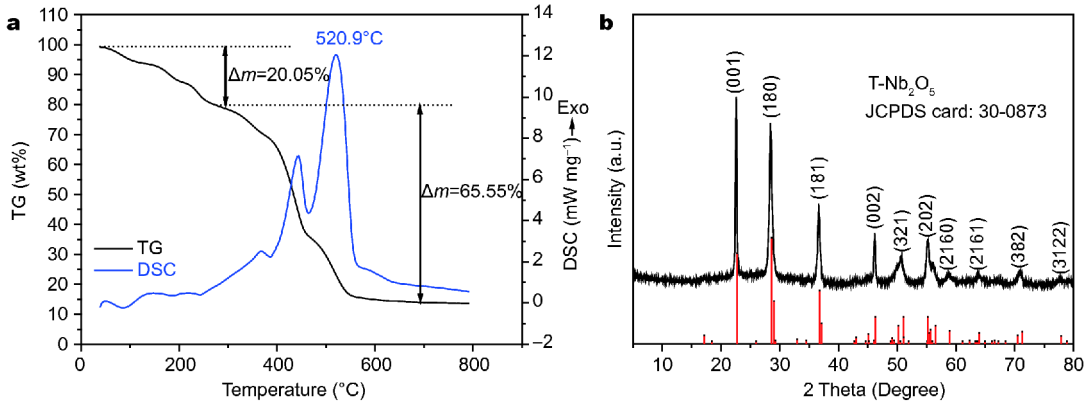

Figure 2 TG and DSC results of the Nb_2O_5 nanofiber precursors from room temperature to 800°C in air with a temperature ramping rate of 10°C min^{-1} (a) and the XRD pattern of the Nb_2O_5 nanofiber after heat treatment (b).

details of the unique porous nanofiber structure. As shown in Fig. 1e, the bright spots on the Nb_2O_5 nanofibers confirm the existence of mesopores, which is consistent with the SEM results. Additionally, a higher magnification image (Fig. 1f) shows that the mesoporous features are throughout the nanofiber and connected with one another. The HR-TEM image of a nanofiber (Fig. 1g) reveals the lattice fringes with d-spacing of 0.245 nm, in agreement with the (181) interplanar distance of the orthorhombic structure of Nb_2O_5. As a comparison, the SEM images of commercial Nb_2O_5 are shown in Fig. S2a, b. The commercial Nb_2O_5 is composed of bulk particles, with a diameter of around 3 μm.

DSC and TG analysis were carried out to investigate the decomposition of precursors during the calcination process, and the results are shown in Fig. 2a. The mass loss mainly results from the elimination of remaining moisture and DMF before 300°C, which adds up to about 20.55%. Between 300 and 560°C, a large mass loss of 65.55% can be observed, which can be ascribed to the decomposition of polymer and niobium oxalates. The DSC curve shows strong peaks at approximately 520°C and 430°C, confirming the decomposition reactions. The weight is stabilized after 600°C, implying that the decomposition is completed. Therefore, 600°C is the optimal annealing temperature for the formation of T-Nb_2O_5 nanofibers. Fig. 2b shows the XRD pattern of the obtained Nb_2O_5 nanofibers after annealing in air at 600°C for 2 h. All the diffraction peaks can be indexed to orthorhombic Nb_2O_5 (space group: *Pbam* (55), JPCDS No. 30-0873). No other residual peaks are detected, indicating a high purity of the obtained Nb_2O_5 nanofibers. Moreover, the high intensity of the diffraction peaks manifests good crystallinity of this Nb_2O_5 product. Fig. S3 shows the XRD pattern of the commercial Nb_2O_5 samples, which has the same type of crystal structure of the as-synthesized mesoporous Nb_2O_5 nanofibers. However, the peak intensity is much higher, suggesting much larger crystallite size.

To characterize the porosity of the Nb_2O_5 porous nanofibers, N_2 adsorption-desorption measurements at 77 K were conducted. The adsorption/desorption isotherm curves (Fig. 3a) display type-IV isotherm with type-H3 hysteresis loop at the relative pressure (P/P_0) ranging from 0.5–1.0, demonstrating the mesoporous texture of the nanofibers [35]. According to the Brunauer-Emmelt-Teller (BET) method, the specific surface area of these mesoporous Nb_2O_5 nanofibers is calculated to be 31.03 $m^2 g^{-1}$, which is higher than that of commercial Nb_2O_5 (3.4804 $m^2 g^{-1}$, Fig. S4). The high surface area of Nb_2O_5 nanofibers can be attributed to its mesoporous 1D structure. Fig. 3b displays the pore-size distribution calculated by the Barrett-Joyner-Halenda (BJH) method, which shows the pores are mainly in the range of 2–30 nm. The unique interconnected-mesoporous structure could shorten diffusion length of charged ions, provide more active sites, and enlarge the contact area of active materials and electrolyte during the electrochemical reactions.

The interconnected-mesoporous Nb_2O_5 nanofibers were further assembled into 2016 coin cells to investigate their lithium storage properties. Fig. 4a depicts the first three successive CV curves of T-Nb_2O_5 electrode in the voltage range of 0.01 to 3.0 V (*vs.* Li/Li^+) at a scan rate of 0.1 mV s^{-1}. For the initial cycle, an evident reduction peak is observed at around 0.85 V and disappears in the subsequent cycles, which can be ascribed to the irreversible phase transformation and the formation of SEI film.

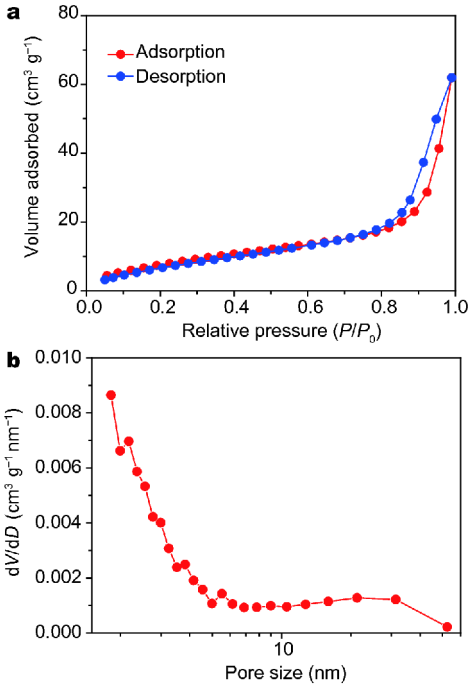

Figure 3 N_2 adsorption/desorption isotherms (a) and Barrett-Joyner-Halenda (BJH) pore size distribution curve (b) of the obtained porous Nb_2O_5 nanofibers.

Another two small reduction peaks located at about 1.84 and 1.50 V could be attributed to the conversion from Nb^{5+} to Nb^{4+} and Nb^{4+} to Nb^{3+}, respectively [36]. The broad oxidation peak at around 2.12 V is corresponding to delithiation process of $Li_xNb_2O_5$. For the second cycle, there is only a broad reduction peak appearing at about 1.68 V, which can be attributed to the lithiation process of Nb_2O_5. Meanwhile, the corresponding oxidation peak is observed to shift to 1.85 V, demonstrating a more efficient lithium-ion extraction process. The almost overlap curves after initial cycle indicates the good electrochemical reversibility of the mesoporous Nb_2O_5 electrode. The detail electrochemical oxidation/reduction reactions can be characterized by the redox reaction as follows: $xLi^+ + xe^- + Nb_2O_5 \leftrightarrow Li_xNb_2O_5$, where x represents the degree of lithium insertion and x varies from 0 to 2 [37,38].

Fig. 4b shows the first three successive CV curves of mesoporous T-Nb_2O_5 electrode in the voltage range of 1.0 to 3.0 V (*vs.* Li/Li$^+$) at a scan rate of 0.1 mV s^{-1}. Similar to 0.01–3 V, the two reduction peaks (1.83 and 1.52 V) result from the Li^+ intercalation, while one oxidation peak (1.82 V) can be ascribed to Li^+ de-intercalation. However, for the initial CV curve in 1.0–3.0 V, the sharp peak below 1.0 V disappeared, suggesting no irreversible phase transformation and formation of SEI film. Besides a slight decrease of reduction peak intensity, no obvious change occurs in the later cycles. It indicates that when the cut-off voltage is operated above 1.0 V, there is almost no SEI film formation upon cycling, which results in a low irreversible capacity loss and high cycling stability.

The galvanostatic charge-discharge profiles for 1st, 2nd, 3rd, 50th, and 100th cycle and the cycling performance curves at the current density of 0.1 A g^{-1} are shown in Fig. 4c and d. When the cut-off was set to 0.01–3.0 V, the discharge-charge profiles (Fig. 4c) are well defined and located at around 1.85 and 1.68 V (except for the first cycle), in agreement with the CV peaks (Fig. 4a). The initial discharge and charge specific capacities are 478 and 336 mA h g^{-1} respectively, indicating an initial coulombic efficiency of 70.3% (Fig. 4e). The large irreversible capacity loss is mainly attributed to the decomposition of electrolyte and the formation of SEI films. After 120 cycles, the reversible specific capacity can still remain 326 mA h g^{-1} (a capacity retention of 68.2%), demonstrating a good cycling stability and high reversible capacity (Fig. 4e). When the cut-off voltage was set to 1.0–3.0 V, the initial discharge and charge specific capacity are 215 and 180 mA h g^{-1}, respectively, indicating an initial cycle coulombic efficiency of 84% (Fig. 4d). Higher coulombic efficiency than that in 0.01–3 V could be ascribed to the absence of irreversible phase transformation and formation of SEI film, which consumed extra Li^+. Thereafter, the coulombic efficiency rises to around 99% and is observed to be stable. After 120 cycles, the reversible discharge specific capacity is 184 mA h g^{-1} (a capacity retention of 87%), demonstrating a high cycling stability and good capacity retention in the voltage range of 1.0–3.0 V. Fig. 4f shows the rate capabilities of mesoporous Nb_2O_5 nanofibers and commercial Nb_2O_5. For mesoporous Nb_2O_5 nanofibers, capacities of 286, 252, 208, 183, 155, and 95 mA h g^{-1} can be achieved at the current densities of 0.1, 0.2, 0.5, 1.0, 2.0, and 5.0 A g^{-1}, respectively, with the voltage range of 0.01–3.0 V. When the current was reset to 0.1 A g^{-1}, the electrode can reach a stable capacity of 280 mA h g^{-1}. By contrast, the commercial Nb_2O_5 electrode only shows specific capacities of 90, 60, 35, 22, 12, and 5 mA h g^{-1} at the current densities of 0.1, 0.2, 0.5, 1.0, 2.0, and 5.0 A g^{-1} in the same voltage range, which are much lower than those of mesoporous Nb_2O_5 electrode. Moreover, when the cut-off voltage was set to 1.0–3.0 V, the porous Nb_2O_5 fibers electrode delivers discharge specific capacities of 204, 203, 192, 172, 139, and 65 mA h g^{-1} at the current densities of 0.1, 0.2, 0.5, 1.0, 2.0, and 5.0 A g^{-1}, respectively. While the current density was reset to 0.1 A g^{-1}, the electrode can recover its

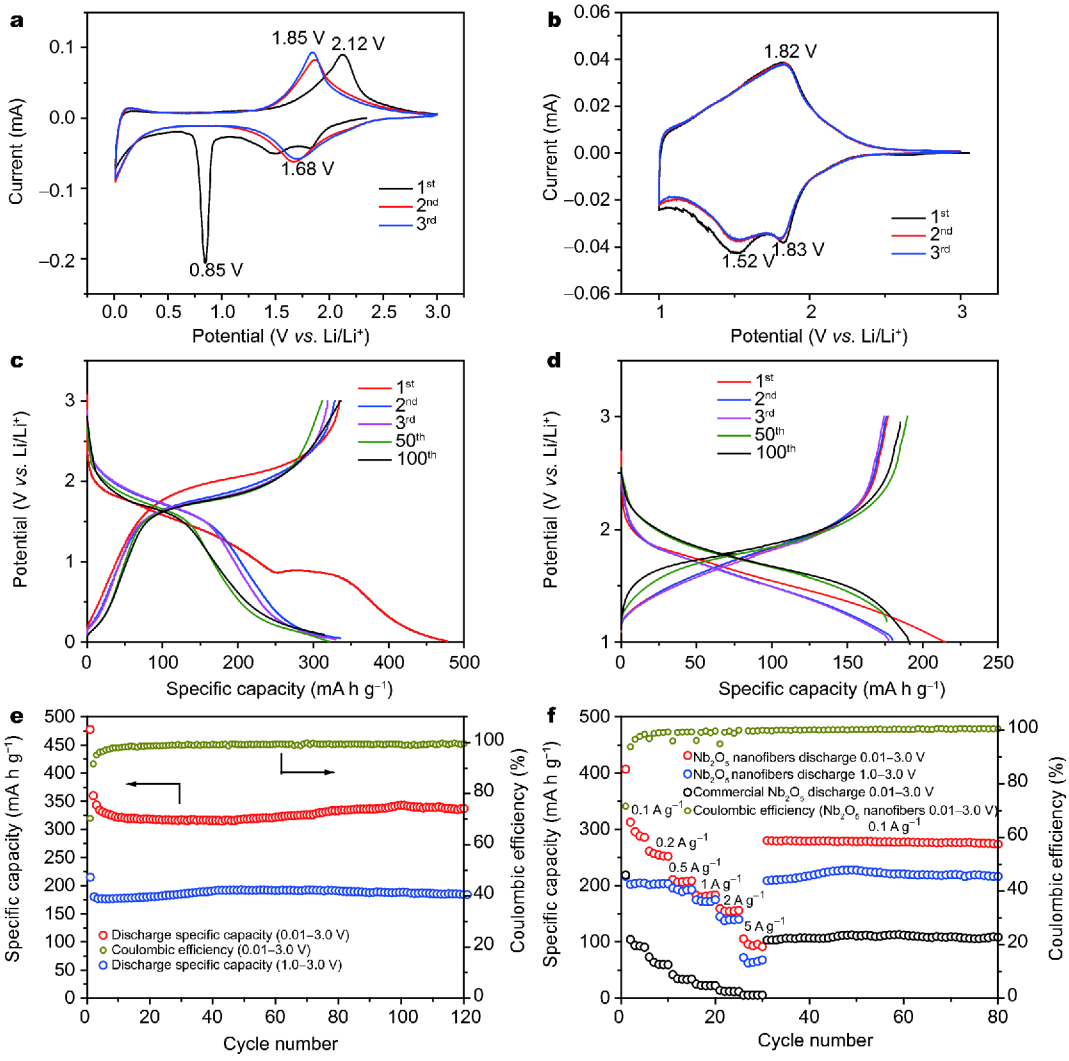

Figure 4 The initial three CV curves of the Nb_2O_5 nanofibers at a scan of 0.1 mV s^{-1} with the voltage ranges of (a) 0.01–3.0 V; (b) 1.0–3.0 V *vs.* Li/Li^+. Galvanostatic charge-discharge profiles of the Nb_2O_5 nanofibers at a current density of 0.1 A g^{-1} with the voltage ranges of (c) 0.01–3.0 V, (d) 1.0–3.0 V *vs.* Li/Li^+; (e) cycle performance of the Nb_2O_5 nanofibers at a current density of 0.1 A g^{-1}; (f) rate performances of the Nb_2O_5 nanofibers and commercial Nb_2O_5, and Coulombic efficiency of Nb_2O_5 nanofibers at different rates.

capacity, even a little higher than the capacity before rate test. These results demonstrate that the mesoporous Nb_2O_5 nanofiber electrode possesses a remarkable rate capability and cycling stability in both 0.01–3.0 V and 1.0–3.0 V.

Fig. 5a shows the long-term cycling performance of the mesoporous Nb_2O_5 nanofibers and the commercial Nb_2O_5 electrode at a current density of 1 A g^{-1}. Both of them have a gradual capacity decrease in the initial several cycles, due to the drastic structural reorganization accompanied by the decomposition and reformation of the electrolyte, which has been described in many previous reports [25,38,39]. For the porous Nb_2O_5 nanofibers at 0.01–3.0 V, the discharge capacity begins to increase in the subsequent cycles. Even after 1,000 cycles, the discharge capacity of porous Nb_2O_5 electrode can still stabilize at ~238 mA h g^{-1}. The increasing discharge capacity can be attributed to the activation processes upon cycling [40,41]. After repeated cycling, the porous structure can be effectively restructured and the SEI layers can be optimized as well. Furthermore, the interconnected mesoporous nanofibers expose many active sites, leading to the increment of capacity in the subsequent cycles [42]. For comparison, the commercial Nb_2O_5 electrode only delivers a stable discharge specific capacity of 40 mA h g^{-1}. Besides, when the voltage range was set to 1.0–3.0 V, the

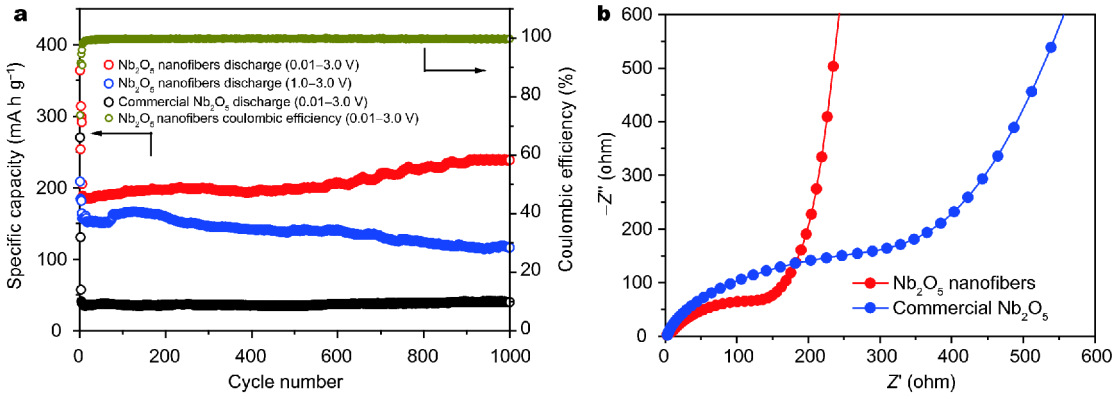

Figure 5 (a) Cycle performances at a current density of 1 A g^{-1}; (b) Nyquist plots of the Nb_2O_5 nanofibers and commercial Nb_2O_5 electrodes, respectively.

Table 1 Comparison of several Nb_2O_5 anode materials used in lithium-ion batteries

Materials	Specific capacity (mA h g^{-1})	Current density (mA g^{-1})	Cycles (n)	Voltage (V)	Ref.
Nb_2O_5 nanofibers	238	1000	1000	0.01–3.0	This work
	166	1000	200	1.0–3.0	
Nb_2O_5 nanobelts	150	100	50	1.0–3.0	[38]
Nb_2O_5 hollow spheres	172	100	250	1.0–3.0	[34]
Nb_2O_5/C	130	200	300	1.0–3.0	[43]
Nb_2O_5 nanosheets	83	1000	200	1.0–3.0	[39]
Nb_2O_5/C nanotube	185	5000	200	0.01–3.0	[36]

capacity fading of porous Nb_2O_5 electrode is detected for the first 80 cycles. Thereafter, the capacity starts to increase and reaches a peak value of 166 mA h g^{-1} before stabilized. After 1,000 cycles, it still delivers a capacity of 118 mA h g^{-1}. Moreover, the porous Nb_2O_5 nanofibers electrode has a much smaller equivalent resistance than the commercial Nb_2O_5 electrode (Fig. 5b). These results demonstrate that the interconnected-mesoporous structure of the obtained Nb_2O_5 nanofibers accelerates the lithium-ion and electrons diffusions and leads to excellent electrochemical performances.

A comparison on electrochemical performances of this work and other previous reported Nb_2O_5 anode materials for LIBs is shown in Table 1. The as-synthesized porous Nb_2O_5 nanofibers deliver higher electrochemical performances than those of previous studies, in terms of both specific capacity and cycling stability.

CONCLUSIONS

In summary, porous Nb_2O_5 nanofibers were successfully fabricated *via* a facile electrospinning method followed by heat treatment. The obtained nanofibers are of high porosity with a diameter of approximately 100 nm. The abundant interconnected mesopores can create well-defined channels for the diffusion of ions and electrons, provide more active sites and facilitate the electrolyte penetration. When used as anode materials for LIBs, the as-synthesized porous Nb_2O_5 nanofibers deliver excellent electrochemical performances at two different voltage ranges (0.01–3.0 V and 1.0–3.0 V), including rate capability and cycling stabilities. These results demonstrate that design of Nb_2O_5 nanofibers with interconnected mesopores is an efficient way to improve the lithium storage properties of Nb_2O_5 materials.

Received 16 July 2018; accepted 9 August 2018; published online 10 September 2018

1 Bruce PG, Scrosati B, Tarascon JM. Nanomaterials for rechargeable lithium batteries. Angew Chem Int Ed, 2008, 47: 2930–2946
2 Hu L, Qu B, Li C, *et al.* Facile synthesis of uniform mesoporous $ZnCo_2O_4$ microspheres as a high-performance anode material for Li-ion batteries. J Mater Chem A, 2013, 1: 5596–5602
3 Wu HB, Chen JS, Hng HH, *et al.* Nanostructured metal oxide-

based materials as advanced anodes for lithium-ion batteries. Nanoscale, 2012, 4: 2526–2542
4 Ji L, Lin Z, Alcoutlabi M, *et al.* Recent developments in nanostructured anode materials for rechargeable lithium-ion batteries. Energy Environ Sci, 2011, 4: 2682–2699
5 Rahman MM, Rani RA, Sadek AZ, *et al.* A vein-like nanoporous network of Nb_2O_5 with a higher lithium intercalation discharge cut-off voltage. J Mater Chem A, 2013, 1: 11019–11025
6 Lei K, Li F, Mu C, *et al.* High K-storage performance based on the synergy of dipotassium terephthalate and ether-based electrolytes. Energy Environ Sci, 2017, 10: 552–557
7 Kong X, Zhu T, Cheng F, *et al.* Uniform $MnCo_2O_4$ porous dumbbells for lithium-ion batteries and oxygen evolution reactions. ACS Appl Mater Interfaces, 2018, 10: 8730–8738
8 Wang Y, Zhu T, Zhang Y, *et al.* Rational design of multi-shelled CoO/Co_9S_8 hollow microspheres for high-performance hybrid supercapacitors. J Mater Chem A, 2017, 5: 18448–18456
9 Tang C, Liu Y, Xu C, *et al.* Ultrafine nickel-nanoparticle-enabled SiO_2 hierarchical hollow spheres for high-performance lithium storage. Adv Funct Mater, 2018, 28: 1704561–1704568
10 Park CM, Kim JH, Kim H, *et al.* Li-alloy based anode materials for Li secondary batteries. Chem Soc Rev, 2010, 39: 3115–3141
11 Du N, Zhang H, Chen B, *et al.* Synthesis of polycrystalline SnO_2 nanotubes on carbon nanotube template for anode material of lithium-ion battery. Mater Res Bull, 2009, 44: 211–215
12 Wu ZS, Ren W, Wen L, *et al.* Graphene anchored with Co_3O_4 nanoparticles as anode of lithium ion batteries with enhanced reversible capacity and cyclic performance. ACS Nano, 2010, 4: 3187–3194
13 Zhang J, Ni S, Tang J, *et al.* The preparation of NiO/C-Ni composite as binder free anode for lithium ion batteries. Mater Lett, 2016, 176: 21–24
14 Xu H, Wang W. Template synthesis of multishelled Cu_2O hollow spheres with a single-crystalline shell wall. Angew Chem Int Ed, 2007, 46: 1489–1492
15 Arunkumar P, Ashish AG, Babu B, *et al.* Nb_2O_5/graphene nanocomposites for electrochemical energy storage. RSC Adv, 2015, 5: 59997–60004
16 Liu Z, Guan D, Yu Q, *et al.* Monodisperse and homogeneous SiO_x/C microspheres: A promising high-capacity and durable anode material for lithium-ion batteries. Energy Storage Mater, 2018, 13: 112–118
17 Rani RA, Zoolfakar AS, O'Mullane AP, *et al.* Thin films and nanostructures of niobium pentoxide: fundamental properties, synthesis methods and applications. J Mater Chem A, 2014, 2: 15683–15703
18 Schäfer H, Gruehn R, Schulte F. The modifications of niobium pentoxide. Angew Chem Int Ed, 1966, 5: 40–52
19 Zhao Y, Zhou X, Ye L, *et al.* Nanostructured Nb_2O_5 catalysts. Nano Rev, 2012, 3: 17631–17641
20 Yan L, Rui X, Chen G, *et al.* Recent advances in nanostructured Nb-based oxides for electrochemical energy storage. Nanoscale, 2016, 8: 8443–8465
21 Kumagai N. Thermodynamics and kinetics of lithium intercalation into Nb_2O_5 electrodes for a 2 V rechargeable lithium battery. J Electrochem Soc, 1999, 146: 3203–3210
22 Kim H, Lim E, Jo C, *et al.* Ordered-mesoporous Nb_2O_5/carbon composite as a sodium insertion material. Nano Energy, 2015, 16: 62–70
23 Wei M, Qi Z, Ichihara M, *et al.* Synthesis of single-crystal niobium pentoxide nanobelts. Acta Mater, 2008, 56: 2488–2494
24 Liu F, Xue D. Fabrication of Nb_2O_5 nanotrees with controlled branching degrees. Phys Scr, 2010, T139: 014074
25 Luo H, Wei M, Wei K. Synthesis of Nb_2O_5 nanosheets and its electrochemical measurements. Mater Chem Phys, 2010, 120: 6–9
26 Varghese B, Haur SC, Lim CT. Nb_2O_5 nanowires as efficient electron field emitters. J Phys Chem C, 2008, 112: 10008–10012
27 Viet AL, Reddy MV, Jose R, *et al.* Nanostructured Nb_2O_5 polymorphs by electrospinning for rechargeable lithium batteries. J Phys Chem C, 2010, 114: 664–671
28 Wu L, Lang J, Wang R, *et al.* Electrospinning synthesis of mesoporous $MnCoNiO_x$@double-carbon nanofibers for sodium-ion battery anodes with pseudocapacitive behavior and long cycle life. ACS Appl Mater Interfaces, 2016, 8: 34342–34352
29 Liu X, Liu G, Chen H, *et al.* Facile synthesis of Nb_2O_5 nanobelts assembled from nanorods and their applications in lithium ion batteries. J Phys Chem Solids, 2017, 111: 8–11
30 Niu C, Meng J, Han C, *et al.* VO_2 nanowires assembled into hollow microspheres for high-rate and long-life lithium batteries. Nano Lett, 2014, 14: 2873–2878
31 Chao D, Xia X, Liu J, *et al.* A V_2O_5/conductive-polymer core/shell nanobelt array on three-dimensional graphite foam: a high-rate, ultrastable, and freestanding cathode for lithium-ion batteries. Adv Mater, 2014, 26: 5794–5800
32 Luo Z, Liu L, Ning J, *et al.* A microporous covalent-organic framework with abundant accessible carbonyl groups for lithium-ion batteries. Angew Chem Int Ed, 2018, 57: 9443–9446
33 Yao Y, Xu N, Guan D, *et al.* Facet-selective deposition of FeO_x on α-MoO_3 nanobelts for lithium storage. ACS Appl Mater Interfaces, 2017, 9: 39425–39431
34 Sasidharan M, Gunawardhana N, Yoshio M, *et al.* Nb_2O_5 hollow nanospheres as anode material for enhanced performance in lithium ion batteries. Mater Res Bull, 2012, 47: 2161–2164
35 Sing KSW. Reporting physisorption data for gas/solid systems with special reference to the determination of surface area and porosity. Pure Appl Chem, 1985, 57: 603–619
36 Shi C, Xiang K, Zhu Y, *et al.* Preparation and electrochemical properties of nanocable-like Nb_2O_5/surface-modified carbon nanotubes composites for anode materials in lithium ion batteries. Electrochim Acta, 2017, 246: 1088–1096
37 Kodama R, Terada Y, Nakai I, *et al.* Electrochemical and *in situ* XAFS-XRD investigation of Nb_2O_5 for rechargeable lithium batteries. J Electrochem Soc, 2006, 153: A583
38 Wei M, Wei K, Ichihara M, *et al.* Nb_2O_5 nanobelts: A lithium intercalation host with large capacity and high rate capability. Electrochem Commun, 2008, 10: 980–983
39 Liu M, Yan C, Zhang Y. Fabrication of Nb_2O_5 nanosheets for high-rate lithium ion storage applications. Sci Rep, 2015, 5: 8326–8331
40 Zhao G, Zhang L, Li C, *et al.* A practical Li ion battery anode material with high gravimetric/volumetric capacities based on T-Nb_2O_5/graphite composite. Chem Eng J, 2017, 328: 844–852
41 Huang C, Fu J, Song H, *et al.* General fabrication of mesoporous Nb_2O_5 nanobelts for lithium ion battery anodes. RSC Adv, 2016, 6: 90489–90493
42 Sun H, Xin G, Hu T, *et al.* High-rate lithiation-induced reactivation of mesoporous hollow spheres for long-lived lithium-ion batteries. Nat Commun, 2014, 5: 4526–4533
43 Li G, Wang X, Ma X. Nb_2O_5-carbon core-shell nanocomposite as anode material for lithium ion battery. J Energy Chem, 2013, 22: 357–362

Acknowledgements The authors are grateful to the financial supports from the Natural Science Foundation of Hunan Province in China (2018JJ1036), and the Innovation Program of Central South University (2017CX001).

Author contributions Lou L and Kong X performed the experiments and wrote the article; Zhu T and Lin J performed the data analysis; Pan A drew up the experimental method. All authors contributed to the general discussion.

Conflict of interest The authors declare no conflict of interest.

Supplementary information Supporting data are available in the online version of the paper.

Linzhen Lou is a postgraduate student in Professor Anqiang Pan's Group and will receive his MSc degree in the School of Materials Science and Engineering from Central South University. His current research interest is niobium-based materials for anode of lithium ion battery.

Xiangzhong Kong is a PhD candidate student in the School of Materials Science and Engineering from Central South University under the supervision of Professor Anqiang Pan. His research interest is silicon-based anode materials for lithium-ion batteries.

Anqiang Pan is currently a full professor in the School of Materials Science and Engineering at Central South University. He worked as visiting students at the University of Washington and Pacific Northwest National Laboratory in 2008 and 2009, respectively. Then he worked at Nanyang Technological University as a Research Fellow in 2011. He has published >100 papers in peer-reviewed journals. His current interests are rechargeable batteries, supercapacitors and catalysts.

简单合成连续介孔结构的T-Nb_2O_5 纳米纤维用作锂离子电池负极

楼林震[1†], 孔祥忠[1†], 朱挺[1], 林建德[1], 梁叔全[1], 刘菲[1], 曹国忠[1,2], 潘安强[1*]

摘要 五氧化二铌Nb_2O_5由于其良好的倍率性能和安全性, 作为锂离子电池负极材料被广泛研究. 但是其固有的低电子电导率在很大程度上限制了其电化学性能的发挥. 在本论文中, 我们通过静电纺丝和后续空气热处理构建了具有连续介孔结构的T-Nb_2O_5纳米纤维. 介孔结构彼此互连, 确保高表面积的同时也促进了电解液的渗透. 当用作锂离子电池负极时在电压窗口为0.01–3.0 V, 电流密度为1 A g^{-1}的条件下, 循环1000圈后可逆比容量达到238 mA h g^{-1}. 即使提高电压窗口到1.0–3.0 V, 在循环200圈后仍然有166 mA h g^{-1}的可逆比容量. 此外, 电极材料还表现出优异的倍率性能. 多孔纳米纤维结构和T-Nb_2O_5独特晶体结构的协同效应, 增大了电极和电解质的接触面积, 改善了电子传导性, 从而使电化学性能得到提高.

